4442 *Chem. Mater.* **2009,** *21,* 4442–4447
DOI:10.1021/cm901015b

CHEMISTRY OF MATERIALS
Article

Synthesis of Electrically Conducting Tin Films by Low-Temperature, Plasma-Enhanced CVD

Dattatray S Wavhal,[†] Swati Goyal,[‡] and Richard B Timmons*,[†]

[†]*Department of Chemistry and Biochemistry and* [‡]*Department of Bioengineering, University of Texas at Arlington, Arlington, Texas 76019*

Received April 13, 2009. Revised Manuscript Received July 28, 2009

Electrically conducting films were synthesized, at room temperature, by plasma enhanced chemical vapor deposition (PECVD) of a mixture of tetramethyltin (TMT) and oxygen. The chemical composition of the films were strongly dependent on the partial pressures of the two monomers, total reactor pressure, and on RF power input. At higher TMT to O_2 ratios, nonconductive polymer-like films were produced. As the relative proportion of O_2 to TMT and power input were both increased, a modest reduction in carbon content of the films is observed, but a dramatic increase in film conductivity is observed, ultimately attaining a value of 1×10^4 S/cm. Although there are relatively small changes in the overall Sn, O, and C atom percents, with changes in these variables, notable changes in atomic bonding and surface morphologies were observed, as documented by XPS and SEM analyses. In particular, increasing film conductivity can be associated with formation of Sn−Sn bonded moieties, coupled with increasing agglomeration of initially formed nanoparticles into an interconnecting, nodular like structure. Additionally, both these effects become increasingly prominent with increasing film thickness. An important distinguishing feature of the present work, with prior studies, is that this high electrically conductive, nondoped, tin-containing film is obtained entirely at low temperature, as no post plasma thermal heat treatment was employed.

1. Introduction

There have been many papers devoted to synthesis and properties of tin containing films, particularly in recent years. Interest in these films is motivated, in most part, by their electrical conductivities and optical properties. Examples of their usage, particularly when doped with In or other elements, include transparent electrodes for flat-panel displays and polymer-based electronics, as recently reviewed.[1] Additionally, tin dioxide is widely used for sensors because it is an n-type semiconductor whose conductivity is generally responsive to the surrounding atmosphere. Recent applications of tin-containing films for sensor applications include detection of various low-molecular-weight gases, examples of which include H_2,[2] CH_3OH,[3] auto exhaust gases,[4] and natural gas and liquefied propane emissions.[5] Interestingly, tin-based films are increasingly employed for various biomolecule electrochemical-based sensor applications, with recent reports detailing studies involving glucose,[6] proteins,[7] dopamine,[8] and imipramine.[9] Included among other applications of these materials are their use as antistatic films,[10] optical filters,[11] and thin film resistors and heat reflectors.[12] Clearly, interest in these films remains strong at the present time.

A remarkably wide range of technologies have been employed in synthesis of these tin-containing films. Examples of methods employed for this purpose include pyrolysis,[13] sputtering,[14] pulsed laser chemical vapor deposition,[15,16] and sol−gel-based processes.[17] One of the most prominently used methods employed has been that of plasma-enhanced chemical vapor deposition (PECVD). The PECVD process involves a low-pressure, nonequilibrium gas discharge, frequently referred to as a "cold plasma". In these prior studies, a relatively volatile tin containing compound is subjected to a plasma

*Corresponding author. E-mail: timmons@uta.edu.

(1) Minami, T.; Miyata, T. *Thin Solid Films* **2008**, *517*, 1474–1477.
(2) Yan, Q.; Tao, S; Toghiani, H. *Talanta* **2009**, *77*, 953–961.
(3) Mbarek, H.; Saadoun, M.; Bessais, B. *Sens. Lett.* **2008**, *6*, 507–510.
(4) Chung, W.-Y. *Sens. Lett.* **2008**, *6*, 942–946.
(5) Kumar, V.; Srivastava, S. K.; Jain, Ki. *Sens. Transducers J.* **2009**, *101*, 60–72.
(6) Liao, C-W; Chou, J-C; Sun, T-P; Hsiung, S-K; Hsieh, J.-H. *J. Electrochem. Soc.* **2009**, *156*, J21–J27.
(7) Yang, X.-Q.; Guo, L.-H. *Anal. Chim. Acta* **2009**, *632*, 15–20.
(8) Kumar, A.; Singh, D.; Goyal, R. N.; Kaur, D. *Talanta* **2009**, *78*, 964–969.
(9) Xu, Xi.; Zhou, G.; Li, H.; Liu, Q; Zhang, S.; Kong, J. *Talanta* **2009**, *78*, 26–32.
(10) Park, S. H.; Son, Y. C.; Willis, W. S.; Suib, S. L.; Creasy, K. E. *Chem. Mater.* **1998**, *10*, 2389–2398.
(11) Ying, T. H.; Sarmadi, A. M.; Hop, C. E. C. A.; Denes, F. *J. Appl. Polym. Sci.* **1995**, *55*, 1537–1551.
(12) Niklasson, G. A.; Ronnow, D.; Stromme Mattsson, M.; Kullman, L.; Nilsson, H.; Roos, A. *Thin Solid Films* **2000**, *359*, 203–209.
(13) Correa-lozano, B.; Comminellis, C.; Battisti, A. D. *J. Electrochem. Soc.* **1996**, *143*, 203–207.
(14) Serini, P.; Briois, V.; Horrillo, M. C.; Traverse, A.; Manes, L. *Thin Solid Films* **1997**, *304*, 113–119.
(15) Chuah, D. G. S.; Fun, H. K. *Mater. Lett.* **1986**, *4*, 274–275.
(16) Davazoglou, D. *Thin Solid Films* **1997**, *302*, 204–210.
(17) Rella, R.; Serra, A.; Siciliano, P.; Vasanelli, L.; Licciulli, G.; De, A. *Thin Solid Films* **1997**, *304*, 339–346.
(18) Chen, X.; Rajeshwar, K.; Timmons, R. B.; Chen, J.-J.; Chen Oliver, M. R. *Chem. Mater.* **1996**, *8*, 1067–1077.

 Published on Web 09/02/2009

discharge to generate thin tin-containing films.[11,18−20] A variety of low molecular tin-containing monomers have been employed for this purpose, including particularly tetramethlytin (TMT) and tin (IV)chloride. It has been amply demonstrated that variations in plasma parameters, such as gas flow rates and pressures, applied power, substrate temperature, and position of the substrate in the reactor, are influential in determination of the film compositions obtained. In many cases, an additional non-tin-containing compound has been added to the discharge in attempts to modify or control the composition and properties of the resultant films. For example, in the case of TMT monomer, many studies have included the addition of O_2 as a reactant to promote enhanced tin oxide formation, while simultaneously reducing the extent of organic polymer content in the film. Alternately, it has also been shown that the hydrocarbon film content can be minimized using a high temperature (usually in excess of 500 °C) postplasma deposition treatment in O_2-containing atmospheres in which some level of film conductivity is usually achieved. The resultant oxidized films may exhibit mirrorlike (metallic) or opaque appearances, and conductivities in the range of 1×10^{-2} to 1×10^{2} to as high as 1×10^{4} S/cm have been reported.

In the present study, we describe synthesis of highly conductive tin films produced via the PECVD approach, using reactant mixtures of TMT and O_2. An important distinguishing feature of the present work, relative to prior studies, is production of highly conductive films without substrate exposure to any elevated temperatures. Thus the present study extends the utility of the PECVD approach to include many heat-sensitive samples. Additionally, under a given set of plasma deposition conditions, a surprisingly strong dependence of conductivities on film thickness was observed. Spectroscopic and microscopic characterization of these films reveal that this increased conductivity with film thickness is associated with uniquely increased Sn−Sn bond content, coupled with important morphological changes in film structures, as documented below.

2. Experimental Section

Plasma polymerization was carried out in a bell jar type reactor[21] using continuous wave 13.56 MHz RF power input. TMT (Sigma-Aldrich, 95%) was freed from oxygen by three freeze−pump−thaw cycles before use. Polished Si wafers were used as substrate for XPS and SEM studies; glass plates (1×1 cm^2) for electrical conductivity measurements; and, KBr crystals for FTIR spectroscopic studies. Additionally, a variety of polymer substrates were coated, including very thin polypropylene film, to document the efficacy of coating heat sensitive samples. After substrates were placed inside the reactor, a background pressure of 1 mTorr was achieved for each run. Initially, oxygen flow was adjusted for the desired flow rate and pressure, followed by introduction of the TMT. It was observed that production of conductive films was obtained only over a limited range of gas pressures, using the monomer ratios and power inputs employed in this study. The specific plasma experimental conditions employed are given in Table 1. Four different sets of samples were prepared, identified as samples TMT2, TMT4, TMT5, and TMT6. The TMT2 film was deposited with higher concentration ratio of TMT to O_2 (7/1) compared to a ratio of 1.4/1 for samples TMT4, 5, and 6. In particular, because it was noted that the samples prepared under the TMT6 conditions exhibited significantly higher electrical conductivity than the other films, a series of samples were prepared in which the thickness of films deposited under the TMT6 conditions were carefully varied from 10 nm up to 80 nm.

The plasma polymerized films were characterized by Fourier transform infrared spectroscopy (FTIR), X-ray photoelectron spectroscopy (XPS), and scanning electron microscopy (SEM). The FTIR spectra were recorded in the transmission mode at a resolution of 4 cm^{-1} using a Bruker Vector 22 FT-IR spectrophotometer. The XPS analyses utilized Al Kα radiation at 1486.6 eV, with a pass energy of 17.90 eV, giving a resolution of 0.60 eV for the Ag ($3d_{5/2}$) standard. The electron flood gun (neutralizer) was generally not employed as most of the films were sufficiently electrically conductive to avoid sample charging, with the exception of film TMT2. The morphology of the films was studied using a ZEISS supra 55 VP scanning electron microscope. Film thickness was determined using a Tencor Alpha Step 200 profilometer. The electrical conductivity of the films was determined using the four probe method, with a KEITHLEY 224 programmable current source. The sheet resistance (R_s) resistivity (ρ), and conductivity (σ) was calculated using the equations:

$$R_S = 4.53\frac{V}{I}, \rho = R_S t \text{ and, } \sigma = \frac{1}{p}$$

where t is the thickness of the film, V is the potential difference, and I is the current.

3. Results

Spectroscopic Characterization. FTIR transmittance spectra of the plasma generated thin films are shown in Figure1. Although qualitative in nature, these spectra nevertheless provide some valuable insights concerning composition of these films. The TMT2 film, produced under a relatively high ratio of TMT to O_2, reveals absorption bands at 2972 cm^{-1} (CH_3), 2908 cm^{-1} (CH_2), 1455 cm^{-1} (CH_3), 1380 cm^{-1} (CH_2), 1186 cm^{-1} (Sn-CH_3), 960 cm^{-1} (C−C), 725 cm^{-1} (Sn−C rocking mode and/or Sn−O−Sn asymmetric stretching), 565 cm^{-1} (Sn−C asymmetric stretching and/or Sn−O stretching bond), and 512 cm^{-1} (Sn−C, stretching).[22] The IR spectra of films TMT4, TMT5, and TMT6 differ somewhat from that of TMT2. For example, the C−H stretching bands between 2900 and 3000 cm^{-1} are significantly reduced. Additionally, the intensity of the absorption at 725 cm^{-1} is decreased, suggesting that a significant contributor to this peak, in the Figure 1a spectrum, was Sn−C vibrations. Also notable is that the absorptions at 565 and 512 cm^{-1}, observed in Figure 1a, are now merged into one single, broad absorption band centered at 525 cm^{-1}, which would also be consistent

(19) Arefi-Khonsari, F.; Bauduin, N.; Donsanti, F.; Amouroux, J. *Thin Solid Films* **2003**, *427*, 208–215.
(20) Hu, J.; Zong, Y.; Wang, Y.-Z.; Foerch, R.; Knoll, W. *Thin Solid Films* **2005**, *472*, 58–63.
(21) Bhattacharyya, D.; Pillai, K.; Chyan, O. M. R.; Tang, L.; Timmons, R. B. *Chem. Mater.* **2007**, *19*, 2222–2229.
(22) Inagaki, N.; Hashimoto, Y. *Polym. Bull.* **1984**, *12*, 437–440.

Table 1. Plasma Parameters, Deposition Rates, and Film Thickness

sample name	gas flow TMT/O_2 (cc/min)	plasma power (W)	total pressure plasma off/on (mTorr)	deposition rate (nm/min)	thickness of film (nm)
TMT 2	2.5×10^2 /0.35×10^2	75	35/155	270	200
TMT 4	0.5×10^2 /0.35×10^2	30	27/44	52	77
TMT 5	0.5×10^2 /0.35×10^2	50	27/47	43	65
TMT 6	0.5×10^2 /0.35×10^2	75	27/50	26	42

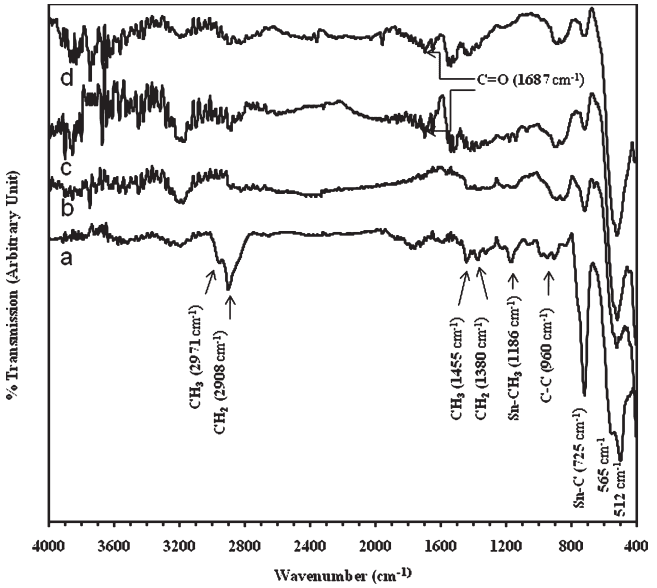

Figure 1. FTIR spectra for films (a) TMT2, (b) TMT4, (c) TMT5, and (d) TMT6.

with possible reduction in Sn−C bonding. The IR spectra of films TMT5 and TMT6 reveal the presence of a weak absorption band at 1687 cm^{-1}, which would be characteristic of oxidized carbon from a carbonyl group, whereas the C−C stretching band at 960 cm^{-1} remains pretty much constant in all four films.

The XPS results provide significantly more quantitative insights into the chemical composition of these films. The elemental composition of films TM2, TMT4 and TMT6 are provided in Table 2, as computed from the C(1s), O(1s), and Sn(3d) XPS peaks. The TMT6 entry actually consists of 6 different films, all produced under the TMT6 conditions shown in Table 1, but differing in film thickness. As shown in Table 2 these film thickness ranged from 10 to 80 nm. The film TMT2 film had [C]/[Sn] and [O]/[Sn] atomic ratios of 1.4 and 1.46, respectively. As the relative concentration of TMT was decreased in the gas mixture, and plasma power input changed from 30W (TMT4) to 75W (TMT6), the atomic ratios of [C]/[Sn] and [O]/[Sn] were also decreased, for example, having values of approximately 0.7 and 1.0 for the sequence of TMT6 films. Although the overall oxygen content of the films remain relatively constant, independent of the monomer ratios or peak power input, the carbon atom content does decrease slightly, whereas that of tin increases in going from the TMT2 sample through the TMT films. This is, of course, a reasonable expectation given the fact that a higher TMT to O_2 ratio was employed during TMT2 film production. Additionally, and somewhat surprisingly, there appears to be a slight,

Table 2. Relative Atom Percentages of the Sn Films from the XPS Spectra

	atom percents			atom ratios	
film name/thickness	C	O	Sn	C/Sn	O/Sn
TMT2	36.2	37.9	25.9	1.40	1.46
TMT4	33.8	35.6	30.5	1.11	1.17
TMT6 (10 nm)	33.5	34.8	31.7	1.05	1.10
TMT6 (20 nm)	30.9	33.5	35.6	0.868	0.941
TMT6 (30 nm)	29.5	36.4	34.1	0.865	1.07
TMT6 (40 nm)	25.9	38.7	35.4	0.732	1.09
TMT6 (60 nm)	26.5	37.3	36.2	0.732	1.03
TMT6 (80 nm)	26.3	37.8	35.8	0.735	1.06

but nevertheless real, decrease in carbon film content as the film thickness was increased for the TMT6 films.

Analysis of the high-resolution Sn ($^3d_{5/2}$) XPS spectral peak provides additional valuable insights concerning the nature of the chemical bonding of the tin atoms in the film, as shown in Figure 2. These deconvoluted spectra have been resolved into four components, located at binding energies of 485 eV (Sn−Sn), 485.8 eV (Sn−C), 486.5 eV (Sn−O), and 487 eV (SnO_2).[23−25] The relative amounts of each of these four components are listed in Table 3. A number of interesting observations can be made with respect to these data. For example, Sn−Sn content is not present in the TMT2 film, whereas significant amounts are observed in the other samples. Furthermore, there is a small, but measurable, increase in the relative amount of Sn−Sn in the TMT6 samples as the film thickness was increased, whereas the amounts of SnO_2 and SnO remain fairly constant.

Microscopic Analysis. SEM analyses of the films deposited on polished Si substrates reveal interesting morphological differences as functions of the deposition conditions employed. In all of the films, clusters of nanosized particles were observed. As shown in Figure 3, the micrographs obtained suggest that film growth incorporates nanosized spherical particles, which agglomerate to form a network. For example, the micrograph of TMT6 10 nm thick film reveals relatively uniform clusters of spherical particles of diameter ranging from 10 to 40 nm (Figure 3a). However, what was quite unexpected, the morphology of the films change markedly with increasing film thickness. As the thickness of the film increased, the spherical particles appear to be increasingly fused together, forming a somewhat elongated nodular structure of length ranging from 20 to 140 nm for the 20 nm thick film (Figure 3b). This aggregation of particles continues with further film thickness increase as the elongated nodular-like structures unite to form what is

(23) Chen, K.-S.; Li, M.-S.; Wu, H.-M.; Yang, M.-R.; Tian, J-Y; Huang, F-Y; Hung, H.-Y. *Surf. Coat. Technol.* **2006**, *200*, 3270.
(24) Larciprete, R.; Borsella, E.; Padova, P. De.; Perfetti, P.; Faglia, G.; Sberveglieri, G. *Thin Solid Films* **1998**, *323*, 291.
(25) Munro, H. S.; Till, C. *Thin Solid Films* **1985**, *131*, 255.

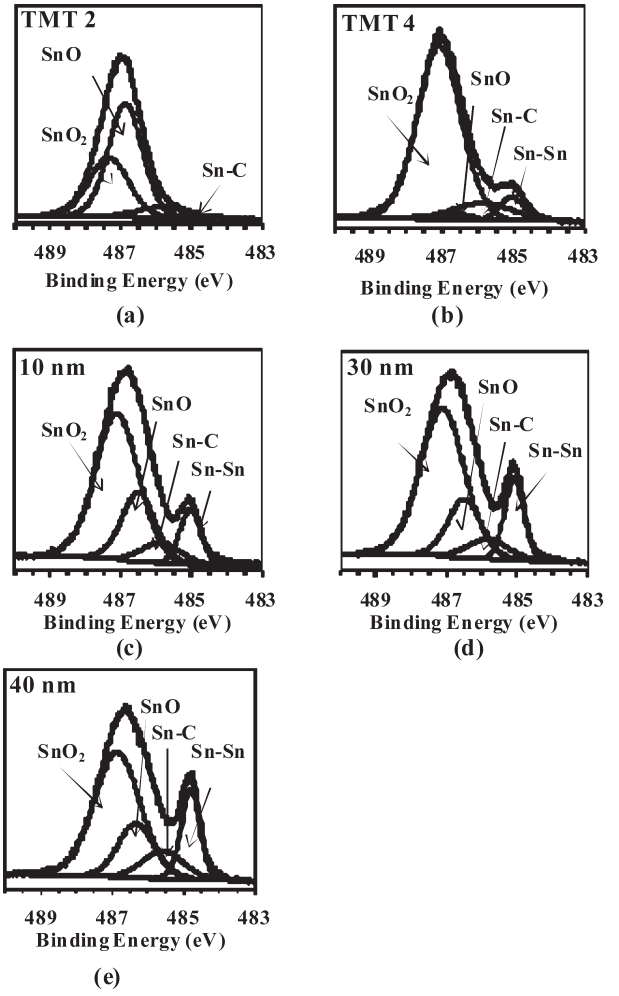

Figure 2. High-resolution, deconvoluted XPS peak of the Sn $^3d_{5/2}$ (a) TMT2, (b) TMT4, (c) TMT6 10 nm (d) TMT6 30 nm thick, and (e) TMT6 40 nm thick.

Table 3. Components of the Deconvoluted Sn ($3d_{5/2}$) High-Resolution XPS peak

	relative % of the Sn-containing moieties			
sample number	SnO_2 (487.00 eV)	SnO (486.5 eV)	Sn−C (485.85 eV)	Sn−Sn (485 eV)
TMT2	80.2	10.3	9.5	00
TMT4	72.2	7.9	10.6	9.3
TMT6 (10 nm)	61.2	21.7	6.9	10.2
TMT6 (20 nm)	60.2	21.8	7.3	10.7
TMT6 (30 nm)	60.5	17.9	7.3	14.3
TMT6 (40 nm)	58.4	19.8	7.2	14.6
TMT6 (60 nm)	57.8	20.6	6.3	15.3
TMT6 (80 nm)	53.1	24.3	6.1	16.5

essentially continuous networks (images c and d in Figure 3). Basically, the same general trend in morphology change with thickness was observed for films deposited on glass substrates.

The morphology of the TMT2 and TMT4 samples (not shown) differed from the TMT6 materials. The TMT2 films were relatively smooth and seemingly devoid of any nanoparticle clusters. The TMT4 film exhibited some clustering of nanoparticles, with size ranging from 20 to 50 nm, but these clusters were not as prominent as those observed with the TMT6 samples.

Electrical Conductivity. The sheet resistance, resistivity, and conductivity of the deposited films are given in Table 4. The electrical conductance of the TMT2 film was so too low to be measured. In contrast, films deposited under higher relative amounts of O_2 exhibited measurable levels of conductivity. The sheet resistance of the TMT4 film was 43 kΩ/□. The TMT6 samples were of higher conductivity and this conductivity was a very sensitive function of film thickness. As shown in Table 4, these samples exhibited a dramatic increase in conductivity with increasing film thickness, with conductivities ranging from. 4.65×10^1 S/cm for the 10 nm film to 1.34×10^4 S/cm for 80 nm thick film.

In light of this strong film conductivity dependence on film thickness, attempts were made to determine the variation in substrate temperatures with increased film deposition times. For this purpose, nonreversible 8-dot thermal sensitive labels, obtained from the Omega Company, were utilized. Heat-sensitive labels having model numbers TL-E-105, and -170, representing strips having melting points ranging from 41 to 116 °C, each 8-dot strip having melting points increasing in increments ranging from 2 to 6 °C, were obtained. The labels were located directly under a thin polypropylene film during the plasma deposition process. The sample temperatures attained by the TMT6 samples, ranging in thickness from 10 to 80 nm, carried out under plasma deposition conditions identical to those listed in Table 1, were observed to increase slowly with film thickness. These values ranged from below 41 °C for the 10, 20, and 30 nm films, to between 41 and 43 °C for the 40 nm film, between 43 and 46 °C for the 60 nm film, and between 49 and 54 °C for the 80 nm sample. The plasma deposition times employed to deposit these films ranged linearly from 20 s for the 10 nm film up to 180 s for the 80 nm thick sample.

X-ray Diffraction. The TMT2, 4, and 6 samples were examined for crystallinity using RXD analysis. Surprisingly, no clear evidence of crystallinity was observed, indicating that these films were completely amorphous in character. It appears that the absence of any high-temperature exposure in the present case is responsible for this lack of crystal formation. For example, in previous work from this lab, the presence of crystalline SnO_2 is clearly documented after thermal treatment of plasma deposited films from TMT.[26]

4. Discussion

The motivation for the present work was to examine the possibility of producing a stable, electrically conductive tin containing film using a simple, low temperature PECVD process. Although, as noted earlier, there have been many reports involving production of thin tin containing films, the tin films exhibiting high electrical conductivity, for example: $\sigma > 1 \times 10^2$ S/cm, have required high temperature exposure, most frequently a post synthesis calcination at $T > 500$ °C. As documented above, plasma deposition of an appropriate mixture of TMT and

(26) Cho, J.; Timmons, R. B. *Chem. Mater.* **2006**, *18*, 2989–2996.

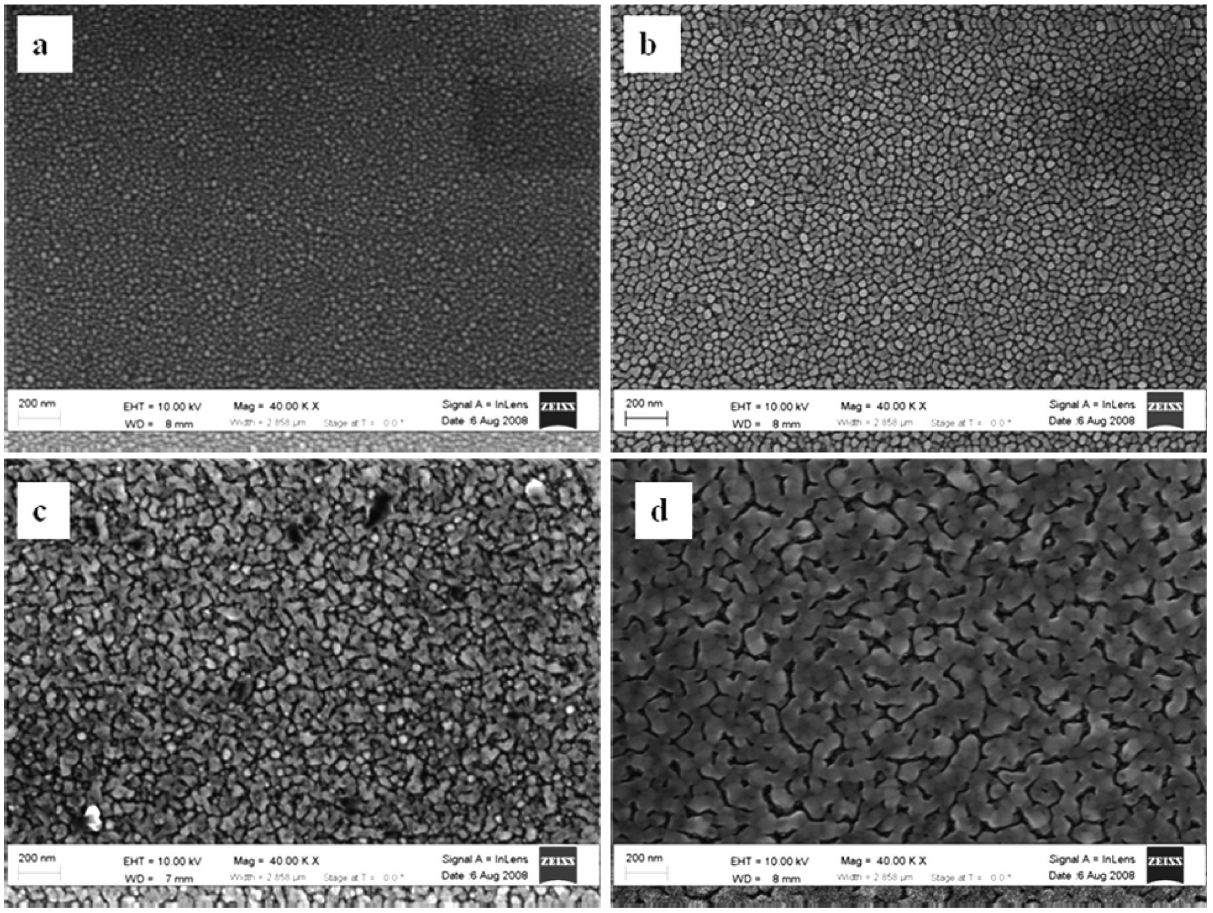

Figure 3. SEM pictures of TMT6 films deposited on Si-wafer as a function of film thickness: (a) 10, (b) 20, (c) 40, and (d) 80 nm, all shown at the same magnification.

Table 4. Electrical Properties of the Films, Immediately after Deposition

film name/ thickness	sheet resistance (R_s) ($\Omega/\square$)	resistivity (Ω cm)	conductivity (S/cm)
TMT2			no conductivity
TMT4	4.30×10^4	3.30×10^{-1}	3.03×10^0
TMT6 10 nm	7.40×10^4	8.88×10^{-2}	4.65×10^1
TMT6 20 nm	1.21×10^4	2.54×10^{-2}	3.93×10^1
TMT6 30 nm	8.60×10^3	2.15×10^{-2}	4.65×10^1
TMT6 40 nm	1.57×10^2	6.61×10^{-4}	1.52×10^3
TMT 60 nm	5.60×10^1	3.17×10^{-4}	3.15×10^3
TMT 80 nm	9.06×10^0	7.43×10^{-5}	1.34×10^4

O_2, carried out at room temperature, can successfully achieve this low-temperature synthesis goal. The elimination of the high temperature step simplifies production of such films in terms of energy and time savings and, more importantly, extends the range of temperature sensitive substrates that can be successfully coated.

At the same time, it is important to note that achieving this goal requires a select combination of plasma deposition variables. Although the plasma conditions shown in Table 1, specifically for the TMT6 samples, were successful in producing the desired film conductivities, many other combinations of reactant variables, including many not presented here, produced high-quality films but none having conductivities comparable to that of the thicker TMT6 films. From our general observations, it appears that the most important plasma parameters in achieving conductive films under low-temperature conditions are the ratio of TMT to O_2, the total reactor pressure (including both with and without plasma ignition), and the power input. For example, although the TMT2 samples produced using a relatively high concentration of TMT involved the highest film deposition rates (Table 1), these films were nonconductive. The higher deposition rate with higher flux of TMT is reasonable in that the TMT serves as the source of the radical species, leading to polymer formation. However, it is interesting to note that although these films contained a significant atom percent of Sn (25.9%), as well as relatively high SnO_2 content (Table 3), they are nonconductive. At lower TMT concentrations, and thus increased relative amounts of O_2, the films begin to exhibit measurable electrical conductivity and, as the power input is increased, the films become increasingly metallic in appearance. In fact, in the case of the thicker TMT6 samples, the films are highly reflective of visible light, ultimately exhibiting a mirrorlike surface for the thicker films.

Although the spectroscopic analyses of these films indicate some changes in elemental film compositions (Table 3), these changes appear to be relatively small considering the dramatic variations in their electrical conductivities (Figure 4). What the FTIR and XPS results do reveal is that the carbon content of these films is converted to a somewhat more oxidized form, relative to Sn−C bonds, under higher O_2 condition and higher

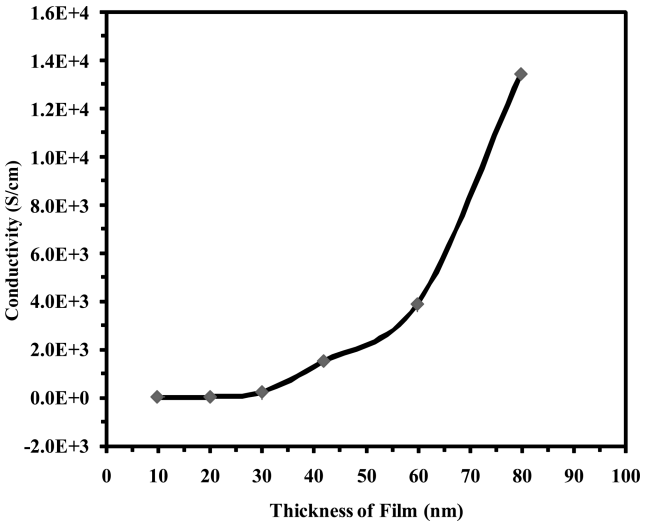

Figure 4. Conductivity of the TMT6 films as a function of film thickness.

power input conditions. For example, as shown in Table 3, the relative Sn−C content is decreased by more than 50% in the TMT6 samples compared to the TMT2 and TMT4 samples. What appears to be far more significant in dictating film physical properties is the appearance of Sn−Sn bonding. This type of bonding is completely absent in the TMT2 sample, is present in the TMT4 sample, is more pronounced in the TMT6 sample, becoming increasingly more prominent as the TMT6 film thickness increases. To the best of our knowledge, this represents the first observation of significant Sn−Sn bonding produced in a low-temperature PECVD process from a volatile tin monomer. Also, as noted earlier, this increased film thickness is accompanied by a clearly changing film morphology. Presumably, this combination of the increasing concentration of conductive Sn−Sn bonds, coupled with the increasingly extended and increasingly interlaced nodular morphology (Figure 3), represents transition through the percolation threshold, ultimately providing a relatively unimpeded, continuous path for electron mobility and thus the high electrical conductivities achieved. It is, however, interesting to reflect on the fact that such large-scale change in physical properties are achieved with relatively small overall changes in elemental compositions. Not only does the conductivity increase sharply with film thickness, but the visual appearance of the films change in that they appear increasingly more metallic in terms of increased reflection, and thus decreased transmission of visible light. Presumably, these increasing metallic properties are the result of the increasing Sn−Sn film content.

At this point, it is not completely clear why the formation of Sn−Sn bonds increase with film thickness for the TMT6 samples. Conceivably, it could arise from a film templating effect associated with the progressively increased aggregation of the initial nanoparticles with higher power input and longer deposition times, as revealed by the SEM studies of these surfaces. Alternately, and seemingly more likely, it arises from the progressively higher substrate temperatures which develop during the higher power input and longer deposition times required for formation of the thicker TMT6 films. As noted earlier, this temperature increase is of the order of at least 10 degrees when comparing the thinner 10, 20, and 30 nm films with the thickest 80 nm thick film.

With respect to potential temperature effects on film compositions, it should be noted that the importance of monomer to oxygen reactant ratios and reactor temperatures on film compositions obtained during PECVD processes have received significant recent attention. Particularly detailed studies are those from Wolden and co-workers examining these variables on formation of a variety of metal oxides.[27−29] As their data clearly document, both the reactant ratios and reactor temperatures are important variables in dictating film compositions obtained under PECVD in dealing with metal oxide systems. For example, reactor temperature was found to exert a strong influence on film structure over the temperature range of 25 to 120 °C during plasma enhanced atomic layering of ZnO.[27] In the present case, the range of increased reactor temperatures are significantly more narrow, but, nevertheless, could have played an important role in the case of the TMT6 films becoming highly conductive. In our case, the slightly increased substrate temperature with increasing deposition time may have been sufficient to promote the slightly increased, but apparently pivotal, abstraction of carbon from the Sn−C groups, required to produce the critical percolation threshold of Sn−Sn content. As shown by the XPS data, the transition of these films from relatively poor conductors to highly conductive is accompanied by a relatively small increase in Sn−Sn bonding (Table 3).

Finally, it is noted that the process developed here was successfully employed to coat a variety of heat sensitive samples. Several polymer samples were treated, including thin, highly flexible polypropylene films. It was possible to deposit strongly adherent, abrasive resistant, conductive (1×10^4 S/cm) films on these polymer substrates. Furthermore, the conductivities of these films were stable over 3 months of measurements and did not change with repeated flexing of the thin polypropylene film.

5. Conclusion

Highly conductive tin containing films can be produced via a low temperature plasma enhanced CVD process in which this conductivity is achieved without having to use post plasma exposure to elevated temperatures. The high electrical conductivity is attributed to the presence of Sn−Sn bonds, coupled with an unusual change in film morphology with increasing film thickness. It will be of interest to determine if similar type observations will exist in PECVD studies of other volatile organometallic compounds.

(27) Rowlette, P. C.; Allen, C. G.; Bromley, O. B.; Dubetz, A. E.; Wolden, C. A. *Chem. Vapor Deposition* **2009**, *15*, 15–20.
(28) Seman, M. T.; Richards, D. N.; Rowlette, P. C.; Kubala, N. G.; Wolden, C. A. *J. Vac. Sci. Technol.* **2008**, *26*, 1213–1217.
(29) Kubala, N. G.; Rowlette, P. C.; Wolden, C. A. *Electrochem. Solid-State Lett.* **2009**, *12*, H259–H262.